

Stacking-Dependent Magnetism in Bilayer CrI₃

Nikhil Sivadas,^{1,*} Satoshi Okamoto,² Xiaodong Xu,^{3,4} Craig. J. Fennie,¹ and Di Xiao⁵

¹*School of Applied and Engineering Physics, Cornell University, Ithaca, New York 14853, USA*

²*Materials Science and Technology Division, Oak Ridge National Laboratory, Oak Ridge, Tennessee 37831, USA*

³*Department of Physics, University of Washington, Seattle, WA98195, USA*

⁴*Department of Materials Science and Engineering,
University of Washington, Seattle, WA 98195, USA*

⁵*Department of Physics, Carnegie Mellon University, Pittsburgh, Pennsylvania 15213, USA*

(Dated: November 19, 2018)

We report the connection between the stacking order and magnetic properties of bilayer CrI₃ using first-principles calculations. We show that the stacking order defines the magnetic ground state. By changing the interlayer stacking order one can tune the interlayer exchange interaction between antiferromagnetic and ferromagnetic. To measure the predicted stacking-dependent magnetism, we propose using linear magnetoelectric effect. Our results not only gives a possible explanation for the observed antiferromagnetism in bilayer CrI₃ but also have direct implications in heterostructures made of two-dimensional magnets.

KEYWORDS : 2D magnets, Moiré superlattices, stacking order, CrI₃, super-superexchange, beyond graphene

Since the demonstration of intrinsic ferromagnetism (FM) in atomically thin crystals [1, 2], there has been a lot of interest in two-dimensional (2D) magnets [3–9]. Among them, CrI₃ presents an intriguing case. While bulk CrI₃ is FM, it becomes a layered antiferromagnet (AFM) when thinned down to a few atomic layers [1]. A number of interesting phenomena associated with this layered antiferromagnetism have been observed, including giant tunneling magnetoresistance when CrI₃ is used as the tunnel barrier [10–12], and gate tunable magneto-optical Kerr effect, along with electrostatic doping control of magnetism [13–16]. However, despite the huge interest, the origin of the AFM interlayer exchange in bilayer CrI₃ remains unclear.

Motivated by the above question, in this Letter we explore the connection between the crystal structure and magnetic properties of bilayer CrI₃ using first-principles calculations. We find that the stacking order defines the magnetic ground state. The coupling of stacking order and magnetism is qualitatively unaffected by atomic relaxation, and is, therefore robust. This stacking-dependent magnetism originates from the competition between orbital-dependent interlayer AFM super-superexchange (SSE) and interlayer FM SSE. Thus, by changing the stacking order one can tune the magnetic ground state between AFM and FM. We also propose using linear magnetoelectric (ME) effect to distinguish between the various predicted AFM stacking orders. In addition to providing a possible explanation for the observed AFM in bilayer CrI₃, our results have a broader impact on other 2D honeycomb magnets such as CrX₃ ($X = \text{Cl, Br, I}$) [17–20] and their heterostructures, including magnetic Moiré superlattices.

As our goal is to understand the stacking dependence of magnetic order in CrI₃, we begin our discussion with the crystal structure of CrI₃. Monolayer CrI₃ consists of

magnetic Cr ions that form a honeycomb lattice, with each Cr atom coordinated by six I atoms that form a distorted edge-sharing octahedron [see Fig. 1 (a), (d)]. Monolayer CrI₃ has the point group D_{3d} . Bulk CrI₃ can be obtained by stacking these monolayer units, which we label as the ‘A’-block [see Fig. 1 (a)]. The bulk has a low-temperature (below 210 K) phase with the space group $R\bar{3}$ and a room-temperature phase with space group $C2/m$ [14, 17, 22]. The low-temperature phase has an ABC-Bernal stacking with each layer laterally shifted by $[2/3, 1/3]$ in fractional coordinates with respect to the neighboring layer. The reduction in symmetry for the high-temperature phase is associated with a relative lateral shift of the stacking order, leaving the monolayer units unaffected [22]. This corresponds to a further lateral shift of $[1/3, 0]$ and $[2/3, 0]$ for the B- and C-monolayer units, respectively, with respect to the ABC-stacking. Thus, both $R\bar{3}$ and $C2/m$ phases have an ABC-stacking sequence. To distinguish the two cases, we refer to the $R\bar{3}$ phase as the ABC-stacking sequence, and the $C2/m$ phase as the AB’C’-stacking sequence. While considering the stacking order in the bilayer, it is, therefore, necessary to consider at least two high-symmetry stacking orders shown in Fig. 1: the AB-stacking (S_6 point group) from the low-temperature bulk structure [see Fig. 1 (b), (e)], and the AB’-stacking (C_{2h} point group) from the high-temperature bulk structure [see Fig. 1 (c), (f)]. Hereafter, the various stacking orders will be discussed with respect to the AB-stacking.

We calculate the total energies using first-principles calculations as implemented in Vienna *ab initio* simulation package (VASP) [23], with the PBEsol functional [24]. A Hubbard on-site Coulomb parameter (U) of 3 eV was chosen for the Cr atoms to account for strong electronic correlations, as suggested by Liechtenstein *et al* [25]. A vacuum region in excess of 15 Å was used

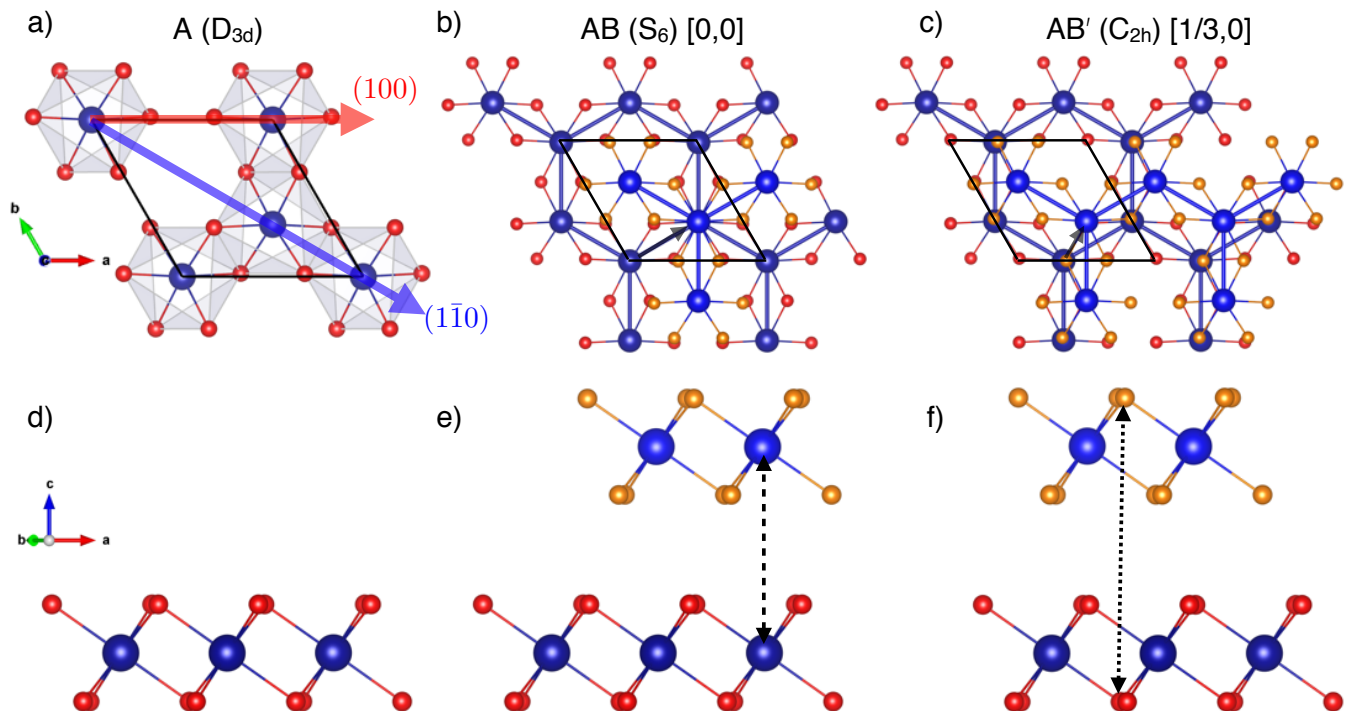


FIG. 1. The crystal structure for different stacking orders of CrI_3 . (a)-(c) The top view, and (d)-(f) the side view of monolayer CrI_3 in (a) and (d), bilayer CrI_3 in AB-stacking in (b) and (e), and bilayer CrI_3 in AB'-stacking in (c) and (f), along with their corresponding point groups. For clarity, the same atoms in the top and the bottom layer are shown by different colors. Blue (dark blue) balls represent the Cr atoms in the top (bottom) layer. Orange (red) balls represent the I atoms in the top (bottom) layer. The Cr-I octahedron is shown only for the monolayer. The high-symmetry $[100]$ - and $[1\bar{1}0]$ - lateral shift directions are labeled in (a) as red and blue translucent arrows, respectively. The honeycomb network of the Cr atoms is shown for the two bilayers in (b) and (c). The relative stacking between the layers is shown by black arrows. AB'-stacking corresponds to a fractional lateral shift of the bottom CrI_3 layer by $[1/3,0]$ with respect to the AB-stacking, and is labeled in (c). The change in the relative stacking order for the lateral shift is shown in (e) and (f) by dashed and dotted lines. The crystal structure is drawn using VESTA [21].

for the bilayer. Structural relaxation was done with a force convergence tolerance of $1 \text{ meV}/\text{\AA}$, in a regular $12 \times 12 \times 1$ Monkhorst-Pack grid with a plane-wave cutoff energy of 450 eV. The computed structural parameters are close to the experimental values for bulk CrI_3 and are listed in the Supporting Information [26]. A stacking-constraint relaxation was performed along the high-symmetry lateral shift directions, relaxing the atomic positions as well as the unit cell volume. We have also verified that the results presented are qualitatively independent of the choice of functional [49]. We make use of ISOTROPY software suite to aid with the group-theoretic analysis [29, 30].

Fig. 2(a) shows the stacking energy defined as the change in energy of the ground state magnetic configuration for a particular stacking order, with respect to the AB-stacking, rigidly shifted along the high-symmetry $[100]$ - (blue dotted line) and $[1\bar{1}0]$ -directions (red solid line). A lateral shift along the $[100]$ -direction corresponds to shifting a monolayer unit along the in-plane projection of the nearest Cr-I bond, whereas, a lateral shift along the $[1\bar{1}0]$ -direction corresponds to shifting a monolayer

unit along the nearest Cr-Cr bond. Naturally, these two directions are inequivalent. The shape of this stacking-dependent energy we find is similar to that of hexagonal boron nitride and graphene along the high-symmetry directions [31–33].

We note that while AB-stacking is at the global minimum, AB'-stacking has energies comparable to AB-stacking and is at a local minimum. A similar result is obtained when the fully relaxed AB'-stacking is used as the reference structure. Hence, even though AB-stacking corresponds to the global minimum, it is conceivable that the bilayer exfoliated at room-temperature is kinetically trapped in this AB'-stacking order, on cooling. This is consistent with the lack of experimental reports of a structural transition on cooling.

We also calculate the interlayer exchange energy defined as the difference in energy between the FM and layered-AFM spin configurations, for each shifted configuration in Fig. 2(a). We find that while AB-stacking strongly prefers FM, AB'-stacking prefers AFM, albeit, weak [see Fig. 2(b)], and is at the phase boundary of FM and AFM [50]. The position of AB'-stacking in the

magnetic phase diagram closer to the FM-AFM boundary is consistent with both the observed giant ME effect [14, 15], and the ease with which the magnetism can be changed by electrostatic doping.

Further, Fig. 2(b) shows a strong coupling between the stacking order and the magnetism. Apart from the bulk-like stacking orders (the AB-stacking and the AB'-stacking orders), we identify other magnetically important stacking orders. While AA-stacking and AB-stacking prefer FM, we find that there are other regions which strongly favor AFM. Among those, there are two symmetry inequivalent stacking orders which have the same point group symmetries as the bilayer from the room temperature phase (AB'-stacking). They are labelled as AC' and AB'₁ in Fig. 2, and corresponds to a fractional lateral shift of the bottom CrI₃ monolayer unit by [2/3,0] and [1/6, -1/6] with respect to the AB-stacking, respectively. Fig. 2(a) suggests that both AC'- and AB'₁-stacking are energetically unfavorable. However, these strong AFM centers are relevant in a Moiré superlattice.

Are there other interesting stacking orders? To answer this we calculated the stacking energy and the interlayer exchange energy for the full 2D space of lateral shifts, by performing a rigid shift of one CrI₃ layer parallel to the basal plane of the second layer, starting with the fully relaxed AB-stacking. A similar result is obtained when the fully relaxed AB'-stacking is used as the reference structure. We have chosen a 6 × 6 grid to perform the lateral shifts. Fig. 2(c) and (d) shows the stacking energy landscape and the interlayer exchange energy landscape, respectively, for the full space of lateral rigid shifts. AB-stacking still remains the global minimum, with AB'-stacking orders having a comparable stacking energy. AB'-, AC'- and AB'₁-stacking orders come in groups of three, as dictated by symmetry [see Fig. 2 (d)]. The strong coupling between the stacking order and the magnetism is also evident. As all the above-identified structures are included in the line-cuts along the [100]- and [110]-directions, we restrict the discussions to these high-symmetry directions, which are representative of the full lateral stacking configuration space.

So far, we have only considered rigid shifts of one monolayer with respect to the other, using fully relaxed AB- and AB'-stacking orders as the reference. Exfoliated thin-films transferred onto a substrate can further relax, retaining the strain and stacking order [34, 35]. Hence, we performed stacking-constraint relaxation along the high-symmetry directions. Fig. 3 shows the effect of this on (a) the stacking energy and (b) the interlayer exchange energy for the high-symmetry [100]- (blue dotted line) and [110]-directions (red solid line). The main effect of the relaxation is to reduce the energies of the high stacking energy configurations, without qualitatively affecting the overall trends [see Fig. 3(a)]. This is accompanied by a change in the interlayer distances (see AC' and AB'₁ in

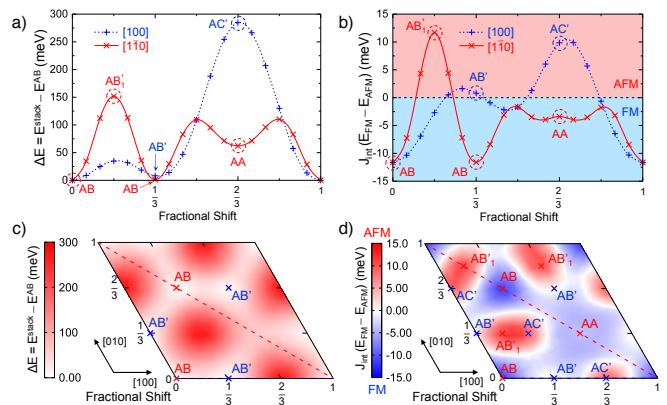


FIG. 2. The stacking energy and the interlayer exchange energy as a function of lateral shift, with respect to the AB-stacking. The stacking energies are shown for (a) the high-symmetry [100]- (dotted blue line) and [110]-directions (solid red line), and for (c) the full space of lateral shifts. The corresponding exchange energy is shown for (b) the high-symmetry [100]- (dotted blue line) and [110]-directions (solid red line), and for (d) the full space of lateral shifts, with positive (negative) regions corresponds to stacking which is AFM (FM). AB'-, AC'-, AA- and AB'₁-stacking orders correspond to a fractional lateral shift of the bottom CrI₃ layer by [1/3,0], [2/3,0], [2/3, 1/3] and [1/6, -1/6] with respect to the AB-stacking, respectively. The heatmaps in (c) and (d) were drawn by interpolating over the neighboring data points on a 6 × 6 grid.

Table I). The relaxed interlayer distances for AB-stacking and AB'-stacking compares well with the bulk experimental interlayer distances [22]. While AB'-stacking remains a local minimum after the relaxation, the energy barriers surrounding it is reduced.

The corresponding effect of the relaxation on the interlayer exchange energies is shown in Fig. 3(b). Similar to the stacking energies, the interlayer exchange energies are qualitatively unaffected. AB- and AA-stacking prefers FM with AB'-, AC'- and AB'₁-stacking preferring AFM, just like in Fig. 2(b). We thus conclude that the stacking order defines the interlayer exchange coupling for the above-identified structures. This strong spin-stacking coupling in bilayer CrI₃ provides a new route to tune the magnetic ground state between AFM and FM.

Next, we discuss the microscopic mechanism of the magnetic coupling. Because the Cr atoms in CrI₃ are in a *d*³ electronic configuration, and the top of the valence band is made up of a combination of the three *t*_{2g} orbitals, the simplest model to describe the magnetism in bilayer CrI₃ includes only the nearest-neighbor intralayer and interlayer exchange interactions [26]. We find that the intralayer exchange is strongly FM (-2.2 meV/μ_B²) and dominates the interlayer exchange which is stacking dependent (0.04 meV/μ_B² for AB'-stacking) [26]. Therefore, CrI₃ bilayers can be viewed as two macroscopic spins

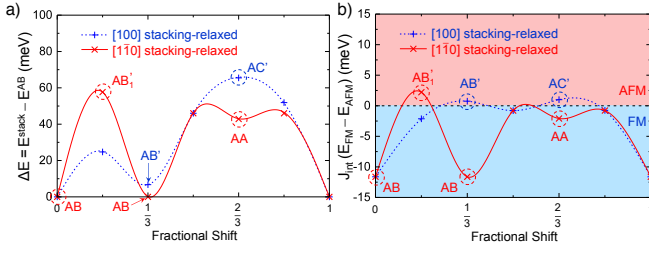


FIG. 3. Effect of stacking-constraint relaxation on (a) the stacking energy and (b) the interlayer exchange energy for the high-symmetry [100]- (dotted blue line) and [110]-directions (solid red line). The identified high-symmetry stacking orders are labeled.

with AFM interactions between them. The energy required to flip a spin involves not only overcoming the interlayer exchange energy but also the intralayer exchange energy as well. This suggests that the Néel temperature for the bilayer should be comparable to the Curie temperature of the monolayer, as reported by experiments [1].

As we are interested in the stacking-dependent magnetism, we focus on the interlayer exchange interaction. Fig. 4(a) shows a schematic of the different exchange interactions between Cr atoms in different layers. Hopping of the form $t_{2g}-t_{2g}$ is prohibited for FM alignment (blue), whereas this is allowed for AFM alignment (red). Therefore, $t_{2g}-t_{2g}$ hybridization leads to AFM. On the other hand, hopping of the form $t_{2g}-e_g$ leads to an exchange coupling that is predominantly FM because of the local Hund coupling [36–38]. All these interlayer Cr-Cr exchange interactions are mediated by the hybridization between the I p orbitals, and therefore, SSE in nature [39]. The stacking-dependent magnetism originates from a competition between the different interlayer orbital hybridizations.

Such a competition is most evident in AB-stacking. The interlayer Cr-Cr nearest-neighbors $J_{1\perp}$ (blue) and the second-neighbors $J_{2\perp}$ (red) for AB-stacking is shown in Fig. 4(b). $J_{1\perp}$ is dominated by virtual excitations between Cr half-filled t_{2g} orbitals, as shown schematically in Fig. 4(c), and induces an AFM coupling [40]. In stark contrast, $J_{2\perp}$ is dominated by a virtual excitation between the Cr half-filled t_{2g} orbitals and the empty e_g orbitals resulting in a net FM coupling, as shown in Fig. 4(d). AB-stacking has one $J_{1\perp}$ bond and sixteen $J_{2\perp}$ bonds per unit cell, as listed in Table I. Hence, the second-neighbor FM interlayer SSE dominates the AFM nearest-neighbor interlayer exchange, making AB-stacking strongly FM [51].

For each stacking order, the ground state magnetism is determined by the competition between the different orbital-dependent AFM and FM exchange interactions. A lateral shift of one monolayer with respect to the other breaks the interlayer hybridization between I p states and generates new ones. This difference is evident while com-

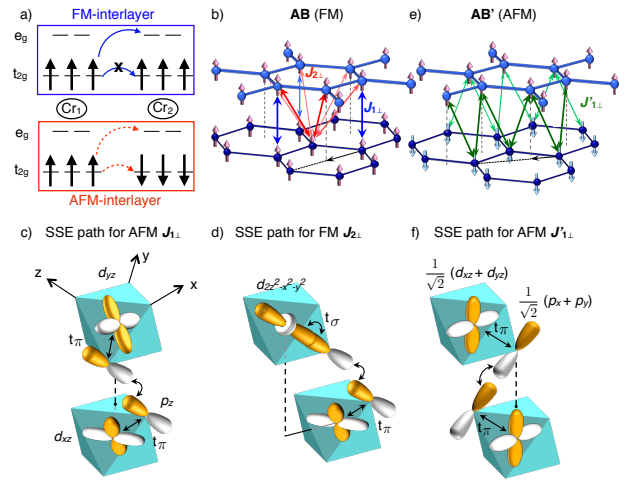


FIG. 4. The interlayer exchange. (a) A schematic of the orbital dependent interlayer SSE interactions. Hopping of the form $t_{2g}-t_{2g}$ is prohibited in FM exchange (blue), whereas this is allowed in AFM exchange (red). The interlayer Cr nearest-neighbor ($J_{1\perp}$, in blue) and the second-neighbor ($J_{2\perp}$, in red) in (b) AB-stacking, and (e) the nearest-neighbor ($J'_{1\perp}$, in green) in AB'-stacking. Schematics for (c) the AFM SSE $J_{1\perp}$ involving half-filled t_{2g} orbitals, (d) the FM SSE $J_{2\perp}$ between half-filled t_{2g} orbital and empty e_g orbital, and (f) the AFM SSE $J'_{1\perp}$ between half-filled t_{2g} orbitals.

paring AB'-stacking [see Fig. 4(e)] to the AB-stacking. For the AB'-stacking, while the nearest-neighbor coordination number is increased compared to the AB-stacking the second-neighbors coordination number is decreased [see Table I]. The combined effect is to reduce the strength of the FM exchange interactions while increasing the AFM exchange, resulting in an AFM ground state for AB'-stacking. Fig. 4(f) shows a schematic of the dominant AFM SSE interaction for AB'-stacking involving the t_{2g} orbitals.

This stacking-dependent magnetism mediated by the I octahedrons is not only applicable to bilayer CrI_3 but also for other octahedrally coordinated 2D-magnets, including CrX_3 ($X = \text{Cl}, \text{Br}, \text{I}$) [17–20]. Further, our results have important implications in the Moiré physics of

TABLE I. The interlayer nearest-neighboring (NN) and second-neighboring distances (2nd-NN) between Cr atoms, with the corresponding coordination number per unit cell in square brackets for the different stacking orders from a rigid shift of the AB-stacking (stacking-constraint relaxed). The shortest interlayer I-I distance is also listed.

Stacking	Cr-Cr NN (Å)	Cr-Cr 2nd-NN (Å)	I-I (Å)
AB	6.7 (6.7) [1]	7.8 (7.8) [16]	4.2 (4.2)
AB'	7.1 (7.1) [6]	8.1 (8.2) [6]	4.2 (4.2)
AC'	7.1 (7.7) [6]	8.1 (8.7) [6]	3.6 (4.3)
AB' ₁	7.0 (7.5) [2]	7.5 (8.0) [8]	3.7 (4.2)
AA	6.7 (7.0) [2]	7.8 (8.0) [10]	4.1 (4.3)

TABLE II. The form of the symmetry allowed linear ME tensor for bilayer CrI₃ for different stacking orders and magnetic orders. The corresponding point group is also labeled in brackets. A linear ME effect is prohibited for all the FM configurations, irrespective of the number of layers and stacking order, as long as inversion is a symmetry of the magnetic space group.

Magnetic and stacking order	Linear ME coefficient
AFM: AB-stacking (S ₆)	$\begin{pmatrix} \alpha_{xx} & \alpha_{xy} & 0 \\ -\alpha_{xy} & \alpha_{xx} & 0 \\ 0 & 0 & \alpha_{zz} \end{pmatrix}$
AFM: AB'-stacking (C _{2h})	$\begin{pmatrix} \alpha_{xx} & 0 & \alpha_{xz} \\ 0 & \alpha_{yy} & 0 \\ \alpha_{zx} & 0 & \alpha_{zz} \end{pmatrix}$
AFM: AA-stacking (D _{3d})	$\begin{pmatrix} \alpha_{xx} & 0 & 0 \\ 0 & \alpha_{yy} & 0 \\ 0 & 0 & \alpha_{zz} \end{pmatrix}$
AFM: General stacking (C _i)	$\begin{pmatrix} \alpha_{xx} & \alpha_{xy} & \alpha_{xz} \\ \alpha_{yx} & \alpha_{yy} & \alpha_{yz} \\ \alpha_{zx} & \alpha_{zy} & \alpha_{zz} \end{pmatrix}$

2D-materials [44–46]. A twisted stacking of bilayers immediately results in regions with spatial variations in the local stacking order. For bilayer CrI₃, the local stacking order defines the length scale of the magnetic Moiré patterns [45]. While both AC'- and AB'₁-stacking were previously identified as energetically unfavorable [see Fig. 2], they form the centers for AFM in the twisted geometry. Similarly, the AB-stacked regions will form the FM centers. Therefore, our results on stacking-dependent magnetism have a direct impact on the Moiré physics of two-dimensional magnets.

Finally, to experimentally verify the predicted stacking-dependent magnetism, and to characterize the magnetic ground state of bilayer CrI₃, we propose the following strategy. Since both time-reversal and inversion symmetry are broken in all AFM configurations, a linear magnetoelectric (ME) effect is allowed by symmetry. But, the specific form of the linear ME tensor $\alpha_{ij} = \partial M_i / \partial E_j$ is determined by the crystalline symmetries itself, and therefore, is strongly dependent on the stacking order. Table II lists the symmetry allowed form for the linear magnetoelectric (ME) effect for these different AFM stacking orders. For instance, the form of the linear ME tensor for AB-stacking and AB'-stacking are very different. While the former allows a toroidal linear ME (α_{xy}) in addition to a transverse linear ME (α_{xx}) and longitudinal linear ME (α_{zz}), the anti-symmetric toroidal term is absent in the latter. Instead, an off-diagonal term, α_{xz} , which is independent of α_{zx} , is symmetry allowed. Thus, by doing a systematic measurement of the various components of magnetization produced in response to a gate-voltage, one can distinguish between the various stacking order in bilayer CrI₃.

In summary, we have shown that magnetism in CrI₃ bilayers is strongly stacking-dependent, and could be

changed between FM and AFM by changing the stacking order. This is a general phenomenon that should exist for a broad class of 2D honeycomb magnets. The sensitive dependence of the magnetic ground state on the local bonding environment suggests great potential for mechanically tuning the magnetism.

NS and CJF are supported by NSF through the Platform for the Accelerated Realization, Analysis, and Discovery of Interface Materials (PARADIM) (DMR-1539918), SO is supported by the U.S. Department of Energy, Office of Science, Basic Energy Sciences, Materials Sciences and Engineering Division, DX and XX acknowledge the support from DOE BES Pro-QM EFRC (DE-SC0019443). The authors thank Kin Fai Mak, Jie Shan, David Muller and Darrell Schlom for interesting discussions and insightful comments. NS thanks Valentino R. Cooper for sharing the input files for bulk CrI₃. NS would also like to thank Gerhard H. Olsen, Betül Pamuk, Matthew W. Daniels, Hena Das and Jisha V.M for various discussions and help with visualization. NS thanks Cornell University Center for Advanced Computing for the computing time.

Note added.—Recently, two related papers [47, 48] have studied the stacking-dependent magnetism in CrI₃ bilayers, but only focused on the AB and AB'-stacking. The stacking-dependent magnetism has also been discussed in the Supplementary Note of Ref. 12.

Supporting Information Available: See Supporting Information for additional structural and magnetism information.

* ns462@cornell.edu

- [1] Huang, B.; Clark, G.; Navarro-Moratalla, E.; Klein, D. R.; Cheng, R.; Seyler, K. L.; Zhong, D.; Schmidgall, E.; McGuire, M. A.; Cobden, D. H.; Yao, W.; Xiao, D.; Jarillo-Herrero, P.; Xu, X. Layer-dependent ferromagnetism in a van der Waals crystal down to the monolayer limit. *Nature* **2017**, *546*, 270 EP –.
- [2] Gong, C.; Li, L.; Li, Z.; Ji, H.; Stern, A.; Xia, Y.; Cao, T.; Bao, W.; Wang, C.; Wang, Y.; Qiu, Z. Q.; Cava, R. J.; Louie, S. G.; Xia, J.; Zhang, X. Discovery of intrinsic ferromagnetism in two-dimensional van der Waals crystals. *Nature* **2017**, *546*, 265 EP –.
- [3] Xing, W.; Chen, Y.; Odenthal, P. M.; Zhang, X.; Yuan, W.; Su, T.; Song, Q.; Wang, T.; Zhong, J.; Jia, S.; Xie, X. C.; Li, Y.; Han, W. Electric field effect in multilayer Cr₂Ge₂Te₆ : a ferromagnetic 2D material. *2D Materials* **2017**, *4*, 024009.
- [4] Lee, J.-U.; Lee, S.; Ryoo, J. H.; Kang, S.; Kim, T. Y.; Kim, P.; Park, C.-H.; Park, J.-G.; Cheong, H. Ising-Type Magnetic Ordering in Atomically Thin FePS₃. *Nano Letters* **2016**, *16*, 7433–7438.
- [5] Seyler, K. L.; Zhong, D.; Klein, D. R.; Gao, S.; Zhang, X.; Huang, B.; Navarro-Moratalla, E.; Yang, L.; Cobden, D. H.; McGuire, M. A.; Yao, W.; Xiao, D.; Jarillo-

- Herrero, P.; Xu, X. Ligand-field helical luminescence in a 2D ferromagnetic insulator. *Nature Physics* **2018**, *14*, 277–281.
- [6] Kim, S. Y.; Kim, T. Y.; Sandilands, L. J.; Sinn, S.; Lee, M.-C.; Son, J.; Lee, S.; Choi, K.-Y.; Kim, W.; Park, B.-G.; Jeon, C.; Kim, H.-D.; Park, C.-H.; Park, J.-G.; Moon, S. J.; Noh, T. W. Charge-Spin Correlation in van der Waals Antiferromagnet NiPS₃. *Phys. Rev. Lett.* **2018**, *120*, 136402.
- [7] Lin, G. T.; Luo, X.; Chen, F. C.; Yan, J.; Gao, J. J.; Sun, Y.; Tong, W.; Tong, P.; Lu, W. J.; Sheng, Z. G.; Song, W. H.; Zhu, X. B.; Sun, Y. P. Critical behavior of two-dimensional intrinsically ferromagnetic semiconductor CrI₃. *Applied Physics Letters* **2018**, *112*, 072405.
- [8] Shcherbakov, D.; Stepanov, P.; Weber, D.; Wang, Y.; Hu, J.; Zhu, Y.; Watanabe, K.; Taniguchi, T.; Mao, Z.; Windl, W.; Goldberger, J.; Bockrath, M.; Lau, C. N. Raman Spectroscopy, Photocatalytic Degradation, and Stabilization of Atomically Thin Chromium Tri-iodide. *Nano Letters* **2018**, *18*, 4214–4219, PMID: 29863369.
- [9] Bonilla, M.; Kolekar, S.; Ma, Y.; Diaz, H. C.; Kalappattil, V.; Das, R.; Eggers, T.; Gutierrez, H. R.; Phan, M.-H.; Batzill, M. Strong room-temperature ferromagnetism in VSe₂ monolayers on van der Waals substrates. *Nature Nanotechnology* **2018**,
- [10] Song, T.; Cai, X.; Tu, M. W.-Y.; Zhang, X.; Huang, B.; Wilson, N. P.; Seyler, K. L.; Zhu, L.; Taniguchi, T.; Watanabe, K.; McGuire, M. A.; Cobden, D. H.; Xiao, D.; Yao, W.; Xu, X. Giant tunneling magnetoresistance in spin-filter van der Waals heterostructures. *Science* **2018**,
- [11] Klein, D. R.; MacNeill, D.; Lado, J. L.; Soriano, D.; Navarro-Moratalla, E.; Watanabe, K.; Taniguchi, T.; Manni, S.; Canfield, P.; Fernández-Rossier, J.; Jarillo-Herrero, P. Probing magnetism in 2D van der Waals crystalline insulators via electron tunneling. *Science* **2018**,
- [12] Wang, Z.; Gutiérrez-Lezama, I.; Ubrig, N.; Kroner, M.; Gibertini, M.; Taniguchi, T.; Watanabe, K.; Imamoglu, A.; Giannini, E.; Morpurgo, A. F. Very large tunneling magnetoresistance in layered magnetic semiconductor CrI₃. *Nature Communications* **2018**, *9*, 2516.
- [13] Sivadas, N.; Okamoto, S.; Xiao, D. Gate-Controllable Magneto-optic Kerr Effect in Layered Collinear Antiferromagnets. *Phys. Rev. Lett.* **2016**, *117*, 267203.
- [14] Jiang, S.; Shan, J.; Mak, K. F. Electric-field switching of two-dimensional van der Waals magnets. *Nature Materials* **2018**,
- [15] Huang, B.; Clark, G.; Klein, D. R.; MacNeill, D.; Navarro-Moratalla, E.; Seyler, K. L.; Wilson, N.; McGuire, M. A.; Cobden, D. H.; Xiao, D.; Yao, W.; Jarillo-Herrero, P.; Xu, X. Electrical control of 2D magnetism in bilayer CrI₃. *Nature Nanotechnology* **2018**, *13*, 544–548.
- [16] Jiang, S.; Li, L.; Wang, Z.; Mak, K. F.; Shan, J. Controlling magnetism in 2D CrI₃ by electrostatic doping. *Nature Nanotechnology* **2018**, *13*, 549–553.
- [17] Handy, L. L.; Gregory, N. W. Structural Properties of Chromium(III) Iodide and Some Chromium(III) Mixed Halides. *Journal of the American Chemical Society* **1952**, *74*, 891–893.
- [18] Bengel, H.; Cantow, H.-J.; Magonov, S.; Hillebrecht, H.; Thiele, G.; Liang, W.; Whangbo, M.-H. Tip-force induced surface corrugation in layered transition metal trichlorides MCl₃ (M?Ru, Mo, Rh, Ir). *Surface Science* **1995**, *343*, 95 – 103.
- [19] Sivadas, N.; Daniels, M. W.; Swendsen, R. H.; Okamoto, S.; Xiao, D. Magnetic ground state of semiconducting transition-metal trichalcogenide monolayers. *Phys. Rev. B* **2015**, *91*, 235425.
- [20] McGuire, M. A.; Yan, J.; Lampen-Kelley, P.; May, A. F.; Cooper, V. R.; Lindsay, L.; Puzos, A.; Liang, L.; KC, S.; Cakmak, E.; Calder, S.; Sales, B. C. High-temperature magnetostructural transition in van der Waals-layered α -MoCl₃. *Phys. Rev. Materials* **2017**, *1*, 064001.
- [21] Momma, K.; Izumi, F. VESTA 3 for three-dimensional visualization of crystal, volumetric and morphology data. *J. Appl. Cryst.* **2011**, *44*, 1272.
- [22] McGuire, M. A.; Dixit, H.; Cooper, V. R.; Sales, B. C. Coupling of Crystal Structure and Magnetism in the Layered, Ferromagnetic Insulator CrI₃. *Chem. Mater.* **2015**, *27*, 612.
- [23] Kresse, G.; Furthmüller, J. Efficient Iterative Schemes for *Ab Initio* Total-energy Calculations Using a Plane-wave Basis Set. *Phys. Rev. B* **1996**, *54*, 11169.
- [24] Perdew, J. P.; Ruzsinszky, A.; Csonka, G. I.; Vydrov, O. A.; Scuseria, G. E.; Constantin, L. A.; Zhou, X.; Burke, K. Restoring the Density-Gradient Expansion for Exchange in Solids and Surfaces. *Phys. Rev. Lett.* **2008**, *100*, 136406.
- [25] Liechtenstein, A. I.; Anisimov, V. I.; Zaanen, J. Density-functional theory and strong interactions: Orbital ordering in Mott-Hubbard insulators. *Phys. Rev. B* **1995**, *52*, R5467–R5470.
- [26] See Supporting Information for additional structural and magnetism information.
- [27] Tkatchenko, A.; Scheffler, M. Accurate Molecular Van Der Waals Interactions from Ground-State Electron Density and Free-Atom Reference Data. *Phys. Rev. Lett.* **2009**, *102*, 073005.
- [28] Bučko, T.; Lebègue, S.; Hafner, J.; Ángyán, J. G. Tkatchenko-Scheffler van der Waals correction method with and without self-consistent screening applied to solids. *Phys. Rev. B* **2013**, *87*, 064110.
- [29] Stokes, H. T.; Hatch, D. M.; J., C. B. ISOTROPY software suite. <http://stokes.byu.edu/isotropy.html>
- [30] Campbell, B. J.; Stokes, H. T.; Tanner, D. E.; Hatch, D. M. ISODISPLACE: a web-based tool for exploring structural distortions. *Journal of Applied Crystallography* **2006**, *39*, 607–614.
- [31] Marom, N.; Bernstein, J.; Garel, J.; Tkatchenko, A.; Joselevich, E.; Kronik, L.; Hod, O. Stacking and Registry Effects in Layered Materials: The Case of Hexagonal Boron Nitride. *Phys. Rev. Lett.* **2010**, *105*, 046801.
- [32] Constantinescu, G.; Kuc, A.; Heine, T. Stacking in Bulk and Bilayer Hexagonal Boron Nitride. *Phys. Rev. Lett.* **2013**, *111*, 036104.
- [33] Popov, A. M.; Lebedeva, I. V.; Knizhnik, A. A.; Lozovik, Y. E.; Potapkin, B. V. Barriers to motion and rotation of graphene layers based on measurements of shear mode frequencies. *Chemical Physics Letters* **2012**, *536*, 82 – 86.
- [34] Lee, J.; Wang, Z.; Xie, H.; Mak, K. F.; Shan, J. Valley magnetoelectricity in single-layer MoS₂. *Nature Materials* **2017**, *16*, 887 EP –.
- [35] Jung, J.; Laksono, E.; DaSilva, A. M.; MacDonald, A. H.; Mucha-Kruczyński, M.; Adam, S. Moiré band model and band gaps of graphene on hexagonal boron nitride. *Phys. Rev. B* **2017**, *96*, 085442.

- [36] Goodenough, J. B. Theory of the Role of Covalence in the Perovskite-Type Manganites $[\text{La}, \text{M}(\text{II})]\text{MnO}_3$. *Phys. Rev.* **1955**, *100*, 564.
- [37] Goodenough, J. B. An interpretation of the magnetic properties of the perovskite-type mixed crystals $\text{La}_{1-x}\text{Sr}_x\text{CoO}_3$?. *J. Phys. Chem. Solids.* **1958**, *6*, 287.
- [38] Kanamori, J. Superexchange interaction and symmetry properties of electron orbitals. *Journal of Physics and Chemistry of Solids* **1959**, *10*, 87 – 98.
- [39] Ehrenberg, H.; Wiesmann, M.; Garcia-Jaca, J.; Weitzel, H.; Fuess, H. Magnetic structures of the high-pressure modifications of CoMoO_4 and CuMoO_4 . *Journal of Magnetism and Magnetic Materials* **1998**, *182*, 152 – 160.
- [40] Anderson, P. W. Antiferromagnetism. Theory of Superexchange Interaction. *Phys. Rev.* **1950**, *79*, 350–356.
- [41] Marzari, N.; Vanderbilt, D. Maximally localized generalized Wannier functions for composite energy bands. *Phys. Rev. B* **1997**, *56*, 12847–12865.
- [42] Souza, I.; Marzari, N.; Vanderbilt, D. Maximally Localized Wannier Functions for Entangled Energy Bands. *Phys. Rev. B.* **2001**, *65*, 035109.
- [43] Mostofi, A.; Yates, J.; Young-See, L.; Souza, I.; Vanderbilt, D.; Marzari, N. Wannier90: A tool for obtaining maximally-localised Wannier functions. *Comp. Phys. Commun.* **2008**, *178*, 685.
- [44] Dean, C. R.; Wang, L.; Maher, P.; Forsythe, C.; Ghahari, F.; Gao, Y.; Katoch, J.; Ishigami, M.; Moon, P.; Koshino, M.; Taniguchi, T.; Watanabe, K.; Shepard, K. L.; Hone, J.; Kim, P. Hofstadter’s butterfly and the fractal quantum Hall effect in moiré superlattices. *Nature* **2013**, *497*, 598 EP –.
- [45] Jung, J.; Raoux, A.; Qiao, Z.; MacDonald, A. H. Ab initio theory of moiré superlattice bands in layered two-dimensional materials. *Phys. Rev. B* **2014**, *89*, 205414.
- [46] Cao, Y.; Fatemi, V.; Fang, S.; Watanabe, K.; Taniguchi, T.; Kaxiras, E.; Jarillo-Herrero, P. Unconventional superconductivity in magic-angle graphene superlattices. *Nature* **2018**, *556*, 43 EP –.
- [47] Jiang, P.; Wang, C.; Chen, D.; Zhong, Z.; Yuan, Z., Z Li; Ji, W. Stacking tunable interlayer magnetism in bilayer CrI_3 . *arXiv:1806.09274* **2018**,
- [48] Soriano, D.; Cardoso, C.; Fernandez-Rossier, J. Interplay between interlayer exchange and stacking in CrI_3 bilayers. *arXiv:1807.00357* **2018**,
- [49] We checked this using PBE-functional with the Tkatchenko-Scheffler correction scheme (DFT-TS) as implemented in VASP [27, 28], and the results are unaffected.
- [50] The magnetic ground state of AB' -stacking is sensitive to the choice of U . For instance, U of 2 eV results in a FM ground state. This is expected given that AB' -stacking is at the phase boundary of AFM and FM.
- [51] We calculated the hopping amplitude for $t_{2g-t_{2g}}$ and the t_{2g-e_g} using first-principles based Wannier90 to explicitly check this [41–43].

